american physiological society

JNP JOURNAL OF NEUROPHYSIOLOGY

J Neurophysiol 134: 1645–1662, 2025.
First published October 18, 2025; doi:10.1152/jn.00431.2025

RESEARCH ARTICLE

Sensory Processing

Neuronal responses to frontal binocular and lateral monocular visual stimuli in the crow nidopallium caudolaterale

Linus Hahner, Lena Hoeppe, and Andreas Nieder

Animal Physiology Unit, Institute of Neurobiology, University of Tübingen, Tübingen, Germany

Abstract

In birds, visual information from the binocular-frontal and monocular-lateral fields is processed through multiple lateralized pathways that converge in associative telencephalic areas, where sensory inputs are integrated to guide behavior. How these initially separated inputs are represented in such higher areas remains unclear. We recorded single-unit activity in the left nidopallium caudolaterale (NCL), a higher-order associative area, in two passively viewing carrion crows (*Corvus corone*). The crows were presented with static and moving sine-wave gratings of varying parameters, and colored natural images, in the frontal binocular and lateral monocular visual fields. About 40% of units were strongly modulated by stimulus position (frontal, left, right), with subpopulations distinguishing frontal versus lateral inputs or left-eye versus contralateral right-eye inputs. Nearly 30% of neurons responded selectively to colored images, whereas only ∼10% discriminated between grating parameters, favoring higher spatial frequencies. Stimulus content interacted with position, showing stronger selectivity for frontal and right-eye inputs, consistent with contralateral processing. These results demonstrate that left NCL integrates inputs from both eyes to represent visual information across the visual fields.

NEW & NOTEWORTHY Single-unit activity recorded in the left associative nidopallium caudolaterale (NCL) of awake crows was modulated by the position of stimuli across the visual field. Distinct subpopulations of visually responsive neurons distinguished both frontal binocular versus lateral monocular inputs and contralateral right-eye versus monocular left inputs. Stimulus content was more consistently encoded in the contralateral half-field, revealing that stimulus processing in left NCL differs across the visual field.

crow; lateralization; nidopallium caudolaterale; single-neuron recording; vision

INTRODUCTION

Flexible behavior requires the mental representation of relevant aspects of an animal's environment. In the visual system of vertebrates, this is achieved via a hierarchy of increasingly sophisticated neuronal computations along parallel brain pathways (1–3). These pathways get integrated in associative areas of the telencephalon that can flexibly adjust behavior based on abstract representations (4, 5). Thus, investigating the neuronal activity in associative areas in response to the visual environment will advance our understanding of how the brain guides behavior.

Visual Pathways in the Avian Brain

Birds are highly visual animals and well-suited to study visual processing from the eyes to the brain. They have outstanding visual acuity and possess excellent color vision (6). The avian brain processes visual information along two major pathways homologous to mammals: The tectofugal pathway is the dominant visual stream in birds and processes information across the whole retina (3). The tectofugal pathway proceeds from the eye via the mesencephalic optic tectum to the diencephalic nucleus rotundus (7, 8). The rotundus sends topographical projections to the entopallium in the endbrain, which in turn projects to various components of the lateral nidopallium (9). Distinct subregions of the rotundus and the entopallium show functional specializations toward different visual features, including color, luminance, and motion (9). The second pathway is the thalamofugal pathway leading from the eye to the lateral geniculate nucleus in the thalamus, and finally to the visual hyperpallium in the endbrain (8). It is involved in processing

Correspondence: A. Nieder (andreas.nieder@uni-tuebingen.de).
Submitted 25 August 2025 / Revised 9 September 2025 / Accepted 3 October 2025

spatial information (10–12) and represents the lateral visual field in pigeons (13). The hyperpallium integrates inputs from both eyes, leading to binocular responses in both plant-feeding and predatory birds (14–16).

Neural Representation of the Frontal and Lateral Visual Fields

Visual processing demands may change across components of the visual field and according to ecological pressures. For birds with laterally placed eyes, a common proposal is that the frontal binocular field serves fine pattern discrimination during near-field vision, e.g., when pecking at grain. By contrast, the lateral monocular fields allow global spatial processing at larger distances, e.g., to localize landmarks, predators, or conspecifics (17). However, such concurrent processes need to be reconciled to guide the behavioral output at any given time point. This sensorimotor transformation occurs in integrative areas of the nidopallium where both visual pathways converge (18). This raises the question of how neural activity at these later stages of visual processing relates to different components of the visual field.

Besides the distinction between frontal and lateral fields, the avian visual system also shows a characteristic degree of lateralization between brain hemispheres (19, 20). At the optic chiasm, the optic nerve of birds fully crosses to the other side. There is also less integration between hemispheres because birds do not have a homolog of the corpus callosum. Interhemispheric integration in the avian brain occurs via different recrossing projections, including the supraoptic decussation and, at the forebrain level, the anterior commissure (21, 22). At the same time, the avian visual pathways show asymmetries in neuronal cell size and in the number of projections from the contralateral hemisphere (19). In pigeons, the left rotundus receives more projections from the contralateral optic tectum than vice versa (23). In the entopallium of chicks, both functional and anatomical asymmetries have recently been reported, favoring the left hemisphere in light-incubated hatchlings (24, 25). Thus, the tectofugal system is lateralized with a more bilateral representation of the visual environment in the left hemisphere (26). By contrast, chicks show a reversed asymmetry of the thalamofugal pathway. Their right hyperpallium receives more contralateral projections from the left thalamus than vice versa, leading to a higher degree of bilateral representation in the right hemisphere (27, 28). How these processing asymmetries shape visual representations in higher integrative areas remains unclear. The telencephalic nidopallium caudolaterale (NCL), which receives input from both tectofugal and thalamofugal pathways (18, 29, 30), is a prime site to address this question.

Integration of Visual Information in NCL

The NCL in birds is an associative endbrain area heavily interconnected with both secondary sensory and premotor areas across modalities (31). It serves as a central executive that can flexibly recruit and update abstract information (32, 33). It is thus a putative functional analog of the mammalian prefrontal cortex (31, 32). In crows, known for their flexible behavior (34), single-cell activity in NCL encodes visuospatial information relevant to immediate goals, including stimulus position (35–37), stimulus features like motion direction and speed (38), and abstract categories like number (39–43). A recent tracing study has shown that the crow NCL receives monosynaptic input from both the visual hyperpallium and the intermediate nidopallium, as well as the entopallial belt (29), suggesting that both thalamofugal and tectofugal signals are integrated in this area. Depending on the asymmetric properties of the ascending visual pathways, these connections may enable NCL to process information from both the left and the right eye. However, physiological studies of the NCL in awake animals usually present visual stimuli only in frontal, binocular positions. It remains unclear how NCL encodes stimuli placed in different parts of the visual field. To address this question, we recorded single-cell activity in the left NCL of two awake carrion crows while simultaneously presenting visual stimuli in the frontal binocular and both lateral monocular visual fields. Our results indicate that left NCL encodes visual information from the ipsilateral eye/contralateral hemisphere to distinguish both contralateral and frontal binocular fields.

METHODS

Animals

We recorded electrophysiological data in two female carrion crows (*Corvus corone*) from the university's facilities: *crow 1* aged 3 yr and *crow 2* aged 1 yr. The crows were kept in social groups in spacious aviaries. During training, crows were kept on a controlled feeding protocol and food was used as reward. The crows always had ad libitum access to water. All procedures were carried out according to the guidelines for animal experimentation of, and approved by, the responsible authority under national legislation, the Regierungspräsidium Tübingen, Germany.

Experimental Setup

Training and data acquisition took place in a closed conditioning chamber (102 × 100 × 76 cm) with a side door. The crows sat on a wooden perch 14 cm in front of a touch screen (3 M. Microtouch, 15 in., 60 Hz refresh rate). On the side walls, 2 additional screens (Joy-it RB-LCD10-2, 10.1 in., 60 Hz refresh rate) were mounted at 35 cm viewing distance each (Fig. 1*A*). Below the front screen, the crows could retrieve food rewards from a custom-made automatic feeder. The task flow was controlled online using the CORTEX program (National Institute of Mental Health). Visual stimuli were presented on the front and side screens, auditory feedback was given by a speaker mounted behind the front screen. The crows' head position was tracked using a custom-written tracking program in MATLAB. This program used the live feed of two infrared vision cameras (Body: FLIR CM3-U3-13y3M, Lens: Fujinon DF6HA-1B, IR-Emitter: Kingbright BL0106-15-28, 940 nm) in the chamber. One camera was mounted on the side wall left to the front screen and tracked the vertical plane, the other was mounted on the top wall and tracked the horizontal plane. The crows had to fixate head position throughout the task by keeping a small reflector attached on top of their head inside of a predetermined area centered between the two side screens. The allowed area for the reflector measured 2.7 cm × 2.7 cm × 2.5 cm, and the head angle had to remain within ±20° of a straight

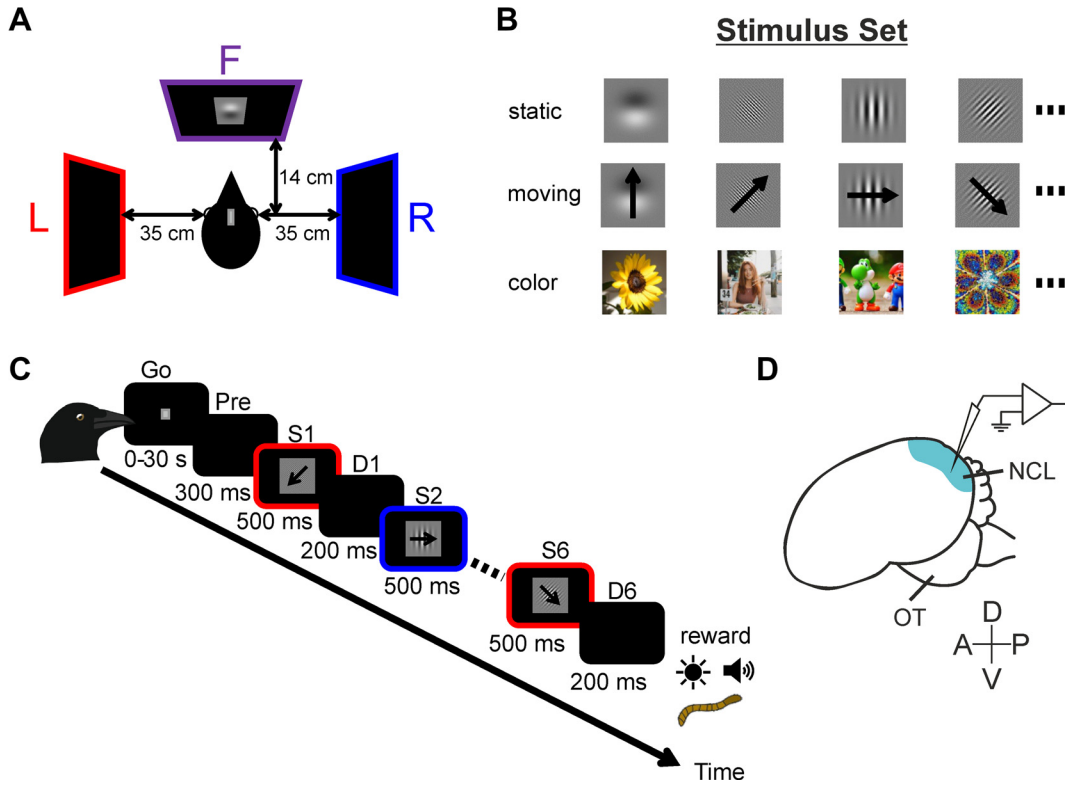

Figure 1. Passive viewing protocol. *A*: screen layout. The crows were surrounded by a frontal and two side screens used for stimulus presentation. Head position was tracked on-line using a reflector attached to the crows' head. *B*: stimulus set. We presented static Gabor gratings with four edge orientations separated by 45° steps and five spatial frequency levels on a logarithmic scale; moving Gabor gratings with eight motion directions separated by 45° steps and the same orientations and frequencies as the static gratings; and 18 different color images. *C*: passive viewing task. An example trial is shown. Crows had to fixate and maintain head position while six stimuli of 500 ms (S1–S6) were presented on varying screens, separated by delays of 200 ms (D1–D6). After the last delay, crows received a food reward and audiovisual feedback. Every trial showed stimuli of the same class, i.e. moving gratings, static gratings or images. Adjacent stimuli always differed in all features. *D*: extracellular recording. Microelectrodes connected to a preamplifier were chronically implanted in the left nidopallium caudolaterale (NCL) of both crows to record single-unit activity. A, anterior; D, dorsal; OT, optic tectum; P, posterior; V, ventral.

forward orientation in the horizontal plane. With these constraints, stimuli presented on either side screen could only be viewed monocularly, whereas stimuli presented in front were within the binocular visual field range of the carrion crow (44).

Stimuli

We presented stimuli sorted into three classes: moving sine-wave gratings, static sine-wave gratings, and colored images (Fig. 1*B*). Stimuli were subsequently shown on the three different screens, so they appeared to the left, to the right, or in front. Stimuli shown on the front screen covered a square area of 3.2 × 3.2 cm, and stimuli shown on either side screen covered a square area of 8 × 8 cm. Thus, all stimuli covered 13° visual angle. Grating stimuli were monochrome, sinusoidal gratings with maximal amplitude, created using a custom-written MATLAB script. We systematically varied spatial frequency, edge orientation, and, for moving gratings, motion direction. Spatial frequency of static and moving gratings was varied by adjusting the number of cycles between a minimum of 1 cycle and the maximum determined by stimulus size and screen resolution. Thus, spatial frequency was 0.077, 0.5, 1, 2, and 2.6 cycles/° for frontal gratings and 0.077, 0.5, 1, 2, and 11 cycles/° for lateral gratings. A horizontal edge orientation of static and moving gratings was labeled as 0°. We then varied edge orientation in 45° steps clockwise, leading to orientations of 0°, 45°, 90° and 135°. For moving gratings, we additionally varied motion direction. Because crows tested with a global motion discrimination task previously showed highest performance for 16°/s motion speed (38), all moving gratings had a fixed speed of 16°/s. This was achieved by adjusting the corresponding temporal frequencies. Motion direction was orthogonal to edge orientation, resulting in two possible directions per orientation. We labeled straight upward motion as 0° and varied motion direction in 45° steps clockwise, leading to motion directions of 0°, 45°, 90°, 135°, 180°, 225°, 270°, and 315°. Stimulus side, motion direction, and spatial frequency were fully balanced, leading to $3 \times 8 \times 5 = 120$ different moving gratings. For static gratings, stimulus side, edge orientation, and spatial frequency were fully balanced, leading to $3 \times 4 \times 5 = 60$ different static gratings. The third class of stimuli consisted of 18 color images randomly selected to provide rich visual information. The full set of images is shown in Supplemental Fig. S1. All images were taken from the stock image platform Pexels (www.pexels.com) and are royalty-free. Total luminance of the images was adjusted to match the luminance of the gratings using a custom-written R-script. All images were shown on all three screens, leading to $18 \times 3 = 54$ different color stimuli. Our combined stimulus set thus consisted of $120 + 60 + 54 = 234$ stimuli in total.

Passive Viewing Task

The basic task flow is shown in Fig. 1*C*. To receive food rewards, crows had to fixate head position throughout individual trials. In each trial, six different stimuli of the same stimulus class were presented in quick succession on the different screens. A trial was initiated by the Go-stimulus, a small gray square shown on the front screen. The Go-stimulus instructed the crows to enter head fixation and stayed onscreen for up to 30 s. When the crow entered fixation, the trial began with a prestimulus phase of 300 ms where all screens remained black. Next, six stimuli separated by brief delay periods were presented. Each stimulus was presented for 500 ms and was followed by a delay of 200 ms during which all screens remained blank. The total set of 234 stimuli was split into 39 trial conditions with a fixed train of six stimuli per condition. All stimuli within a given condition belonged to the same stimulus class, i.e., moving gratings, static gratings, or color images. Parameters varied between stimuli were side, spatial frequency, edge orientation, and motion direction for moving gratings; side, spatial frequency, and edge orientation for static gratings; side and image content for color images. Stimuli were assigned pseudo-randomly such that all varied parameters differed between adjacent stimuli. For instance, a moving grating was always followed by a moving grating shown on a different screen and with different spatial frequency and motion direction. Across conditions, stimulus order was balanced pseudo-randomly such that any given feature was presented at all possible timepoints. The specific stimulus sequence of each condition remained constant across recording sessions throughout the entire experiment. If the crow maintained fixation for the total trial duration of 4,500 ms, the feeder was briefly lit up and delivered a food reward, accompanied by a reward sound from the speaker. Reward delivery was followed by a minimum of 400 ms of eating time. If the crow broke fixation at any point during a trial, this trial was interrupted and a green flash was shown on all screens for 300 ms, followed by a timeout with blank screens of 1,000 ms before a new trial was initiated. The same occurred if the crow did not initiate fixation within 30 s after onset of the Go-stimulus. Trials were separated by an intertrial interval of 200 ms. This interval separated the preceding reward or timeout from the Go-stimulus of the next trial. Trial conditions were drawn pseudo-randomly following a delayed-retry protocol such that interrupted trials were drawn again later until all conditions were presented fully once. Then, a new block of all 39 conditions followed. After every 60 completed trials, crows had a short break with free access to water. Crows completed up to 420 trials per recording.

Surgery and Single-Cell Recordings

Once both crows reliably completed at least 390 trials per day, we implanted custom-made microdrives carrying electrodes for electrophysiological recordings. All surgeries were performed while the animals were under general ketamine/xylazine anesthesia (45). The head was placed in a stereotaxic holder that was customized for crows with the anterior fixation point, the beak bar, at a 45° angle below the horizontal axis of the instrument. Using stereotaxic coordinates (center of craniotomy: anterior-posterior +5 mm relative to interaural point as zero; medial-lateral 13 mm relative to midline), we chronically implanted two microdrives with four electrodes each in the left hemisphere and a connector for the head stage. Glass-coated tungsten microelectrodes with 2 MΩ impedance (Alpha Omega) were used. The electrodes targeted the corvid NCL, which is characterized by dopaminergic cells and has been histologically verified before (46). Crows received analgesics after surgery. When the crows had fully recovered, we recorded single-unit activity while the crows performed the passive viewing task. We recorded from the left hemisphere of both crows, with 45 recording days for *crow 1* and 32 recording days for *crow 2*. Recordings took place between February and May 2024. Every session, the birds were placed in the recording setup and a head stage containing a preamplifier was plugged into the connector implanted on the bird's head and connected to a second amplifier/filter and a PLEXON MAP box outside of the setup by a cable above and behind the bird's head (all components by Plexon Inc., Dallas, TX). Each recording session started with advancing the electrodes until a proper neuronal signal was detected. Neurons were never preselected based on task responsiveness. PLEXON's Offline Sorter was used to manually sort spikes offline into single-unit waveforms.

Data Analysis

We selected single units for statistical analysis based on two inclusion criteria: first, we only analyzed units with an average firing rate of at least 0.5 Hz, calculated as the mean activity over the entire trial length, across all trials recorded. Second, we only included units that were recorded for at least five repetitions of each individual stimulus. We included all stimuli that were fully presented with ongoing head fixation, independent from whether the trial was interrupted later or not. This resulted in a total of 181 units for *crow 1* and 209 units for *crow 2* included in the statistical analysis. All tests had an α level of 5% unless stated otherwise.

Neuronal Selectivity for Visual Features

We analyzed neuronal selectivity to visual features both between- and within stimulus classes: between stimulus classes, we assessed responses to the different classes (moving gratings, static gratings, color images) across the visual field (left screen, front screen, right screen) by applying a two-factor sliding-window ANOVA to all units. For this, we aligned neuronal responses to single stimulus presentations by stimulus onset (=0 ms). We calculated the mean firing rate per stimulus in a 200 ms boxcar window that was shifted in 10-ms steps. For each 10-ms bin, we applied a two-factor ANOVA on the corresponding firing rates. For this, we used the three-level factors of stimulus class (moving, static, color) and stimulus side (left, front, right). Units were identified as stimulus-selective, side-selective, and/or as interaction units when they showed a P value of 0.01 or less for the respective factor for at least 11 consecutive time bins, starting at least 50 ms after stimulus onset to account for visual processing latency. Because both crows showed similar proportions of selective units (Fig. 2*E*), units were pooled across crows for subsequent analyses.

Within each stimulus class, we also applied the sliding-window ANOVA to identify units selective for individual

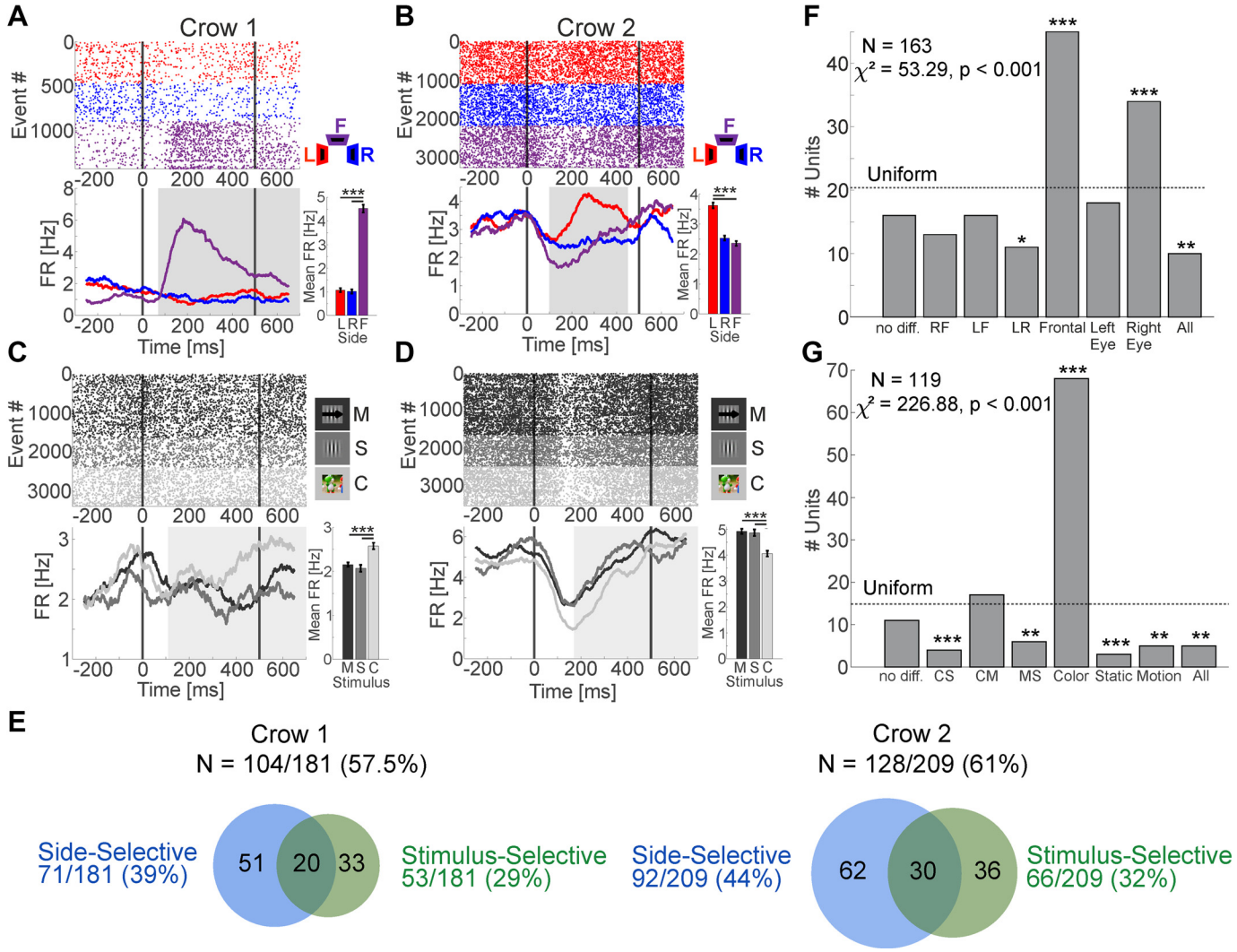

Figure 2. Single nidopallium caudolaterale (NCL) units encode stimulus position and class. *A*: side-selective response to frontal stimuli of an exemplary unit in *crow 1*. *Top*: dot-raster plot of responses to stimulus events over time, aligned by stimulus on- and offset (black lines). Events are grouped and color-coded by position. Each row corresponds to a single event, i.e. a single presentation of a 500-ms stimulus. Each dot indicates an action potential. *Bottom*: spike density curves per side over time. Firing rates were averaged across events and smoothed with a 100-ms boxcar window. Gray shading marks the time window of selective side tuning as determined by a sliding-window ANOVA. *Bottom right*: mean tuning in selective time window. Error bars indicate the means ± SE. ***$P < 0.001$, unpaired *t* test, Bonferroni-corrected. *B*: side-selective response of an exemplary unit in *crow 2*. *C*: stimulus-selective response of an exemplary unit in *crow 1* (*C*) and crow 2 (*D*). Stimulus events are grouped and color-coded by stimulus class. Conventions as in *A* and *B*. Firing rates were increased (*C*) or decreased (*D*) in response to color images compared with sine-wave gratings. *N* = number of selective units among all analyzed units (sliding-window ANOVA). *E*: proportions of side- and stimulus-selective units in *crow 1* (*left*) and *crow 2* (*right*). *F*: distribution of response profiles of side-selective units ($N = 163$, Crows pooled). Units were assigned response profiles based on post hoc pairwise comparisons of sides. Overrepresented profiles were "Frontal," meaning different activity for front vs. side stimuli, and "Right Eye," meaning different activity for right and front vs. left stimuli. The dotted line marks the average number of units per profile expected from a uniform distribution. *$P < 0.05$, **$P < 0.01$, ***$P < 0.001$, Binomial test against chance. *G*: response profiles of stimulus-selective units ($N = 119$, Crows pooled). Conventions as in *F*. The majority of units showed the "Color" response profile, meaning different activity for color images vs. either type of grating. CM, significant difference only between color and motion; CS, significant difference only between color and static; MS, significant difference only between motion and static.

features. For the static gratings, we used a three-way ANOVA with the factors Side, Spatial Frequency, and Edge Orientation. For the moving gratings, we used a nested four-way ANOVA with the factors Side, Spatial Frequency, Edge Orientation, and Motion Direction, where Motion Direction was nested inside Edge Orientation. For the color images, we used a two-way ANOVA with the factors Side and Image at an α level of 1%.

Next, we analyzed the main effects of stimulus class and stimulus side by performing post hoc pairwise comparisons. For this, we compared factor levels within selective units using the mean firing rates in the units' respective selectivity window and applied Bonferroni-corrected unpaired *t* tests at an α level of 1%. Per factor, units could be sorted by response type according to post hoc differences, leading to a distribution of the whole population of selective units across eight possible response selectivities. This categorical distribution was tested against a random uniform distribution using a χ^2-test. In addition, each response selectivity was compared against chance level with a binomial test.

Because of the circular nature of motion direction, we controlled our factorial analysis of moving gratings using circular statistics: first, we tested all units for selective responses to motion direction in a fixed 500-ms window shifted 150 ms relative to stimulus onset. To balance the unequal number of observations per direction, we drew random subsets of 50 stimulus events per direction and calculated the total number of spikes across all drawn events. In cases where there were less than 50 recorded events, we drew events with replacement. The average number of spikes per direction was estimated from 1,000 redraws following this procedure and rounded to the next integer. We performed a Rayleigh test for circular uniformity on this average distribution. We then repeated this analysis separately for each side to control whether position influenced the frequency of direction-selective responses. We extracted spike counts per stimulus event for all units, separately for left, frontal, and right stimuli. For this, we drew 20 stimulus events per side and direction with replacement. The average number of spikes per side and direction was estimated from 1,000 redraws and rounded to the next integer. The Rayleigh test was performed separately for each side. We calculated all circular statistics using the CircStat Toolbox for MATLAB (47).

Side Interactions

To assess interactions of stimulus class and side, we first calculated side indices for the main response selectivity of stimulus-selective units. We compared firing rates to the preferred stimulus class between any two sides A and B with the formula:

$$SI_{AB} = \frac{FR_A - FR_B}{FR_A + FR_B}.$$

This resulted in a side index SI_{AB} normalized between −1 and 1, where negative values indicate relatively stronger responses to the preferred stimulus class on side B, and positive values indicate stronger responses to the preferred stimulus class on side A. Next, we tested for all side pairs whether the distribution of side indices across stimulus-selective units deviated from zero, using t tests for normally distributed values and Wilcoxon signed-rank tests for non-normal distributions. Normality of distributions was assessed by a prior Lilliefors test. This analysis was done separately for units preferring gratings over images versus units preferring images over gratings.

Next, we analyzed units with a significant stimulus interaction in a simple-effects analysis. For this, we compared average firing rates (FRs) between stimulus classes in the interaction window separately for each side. Again, we assessed the response selectivity of all interaction units per side using Bonferroni-corrected unpaired t tests at an α level of 1%.

Finally, to assess whether selectivity to specific feature dimensions differed between sides, we tested all recorded units for feature tuning separately for each side. We calculated average FRs per unit and per side in response to grating stimuli in a 500-ms window starting 150 ms after stimulus onset. We then applied a 1-factorial Kruskal-Wallis test for the different spatial frequencies, edge orientations, and motion directions. For each factor, we then compared population responses between sides with a χ^2-test of the number of selective units per side.

Classifier Analysis

To determine the information content of the activity of the recorded population, we trained a multi-class support-vector machine (SVM) classifier to decode both stimulus class and side. First, we calculated mean FRs of all units to all stimuli in a 500-ms window starting 150 ms after stimulus onset. We then calculated z-scores per unit to train and test the classifier using sixfold cross-validation. To compare classification accuracy to chance level, we trained a random SVM model using the same procedure but with randomly shuffled stimulus labels. We redrew shuffled labels and trained the random model 1,000 times to obtain Monte-Carlo P values for both stimulus class and side. Finally, we trained separate classifiers with the same approach to decode stimulus class per side to investigate if stimulus decoding differed between sides.

RESULTS

We recorded extracellular single-unit responses in the left nidopallium caudolaterale (NCL) of two awake crows while presenting visual stimuli in a passive-viewing protocol (Fig. 1). We presented stimuli on the left, on the right, and in front of the crows' head while they actively maintained a stable head position (Fig. 1*A*). The requirement of a stable head position ensured that stimuli shown on either side screen could only be seen monocularly, whereas stimuli shown on the front screen were seen binocularly. We presented three stimulus classes: static sine-wave gratings, moving gratings—with varying spatial frequency, edge orientation, and motion direction—and complex color images (Fig. 1*B* and Supplemental Fig. S1).

Single NCL Units Encode Stimulus Position and Class

We first analyzed whether single units selectively responded to different stimulus positions (left, front, right) and different stimulus classes (static grating, moving grating, image). For this, we performed a time-resolved sliding-window two-factor ANOVA with the factors "side" and "stimulus" for all units (Supplemental Fig. S2). Examples of side- and stimulus-selective units are shown in Fig. 2, *A–D*. In both crows, large proportions of units showed a main effect of side (*crow 1*: 71 of 181, 39%; *crow 2*: 92 of 209, 44%) and/or a main effect of stimulus (*crow 1*: 53 of 181, 29%; *crow 2*: 66 of 209, 32%). Because both crows showed similar proportions of side-selective and stimulus-selective units (Fig. 2*E*), we pooled units across crows for further analysis. We used the onset of selective coding, relative to stimulus onset, to estimate response latencies of side-selective units. Median response latency was 150 ms (Supplemental Fig. S3), aligning well with previous measures of visual latency in the crow NCL (48).

Left NCL Integrates Visual Information from Both Eyes

We performed post hoc pairwise comparisons of the firing rates of selective units for all combinations of side or stimulus (unpaired t test, $P < 0.01$, Bonferroni-corrected). This resulted in a categorical distribution over eight possible response selectivities for both side- and stimulus-selective units. The distribution of side-selective units was significantly different

from a uniform distribution (Fig. 2*F*, $n = 163$, $\chi^2 = 53.3$, $P < 0.001$).

Most of these units fell into two response selectivities: 28% of side-selective units distinguished frontal binocular from lateral monocular stimuli ("Frontal," 45 of 163 units, $P < 0.001$, binomial test). These units did not respond differently between left and right stimuli, but they distinguished frontal binocular stimuli from lateral monocular stimuli. An example for this profile is the unit in Fig. 2*A*. Comparing FRs across sides revealed an equal split between units with increased activity for frontal over lateral stimuli (22 of 45 units, 49%) and units with increased activity for lateral over frontal stimuli (23 of 45 units, 51%).

In addition, 21% of side-selective units distinguished stimuli seen by the right eye from monocular stimuli seen only by the left eye ("Right Eye," 34 of 163 units, $P < 0.001$, binomial test). Interestingly, these response selectivities sometimes resulted from divergent modulations for both hemifields. For instance, the right-eye unit shown in Fig. 2*B* decreased its FR for frontal and right stimuli but increased FR for left stimuli. This shows that both excitatory and inhibitory responses occurred within units, depending on stimulus position. Thus, left NCL units integrated inputs from both the ipsi- and contralateral eye to distinguish different parts of the visual field.

Stimulus-selective units mainly distinguished between sine-wave gratings and color images. Again, the distribution of stimulus-selective units across response selectivities was nonuniform (Fig. 2*G*, $n = 119$, $\chi^2 = 226.9$, $P < 0.001$). The majority of stimulus-selective units, 57%, showed the same response selectivity ("Color," 68 of 119 units, $P < 0.001$, binomial test). These units responded differently to color images than to either type of grating, but did not distinguish between moving and static gratings. The majority of these units, 71% (48/68), showed higher firing rates for color images than for gratings.

Stimulus-Selective Responses Depend on Position in the Visual Field

Next, we investigated whether single-unit activity in response to different stimuli was modulated by stimulus position. For this, we compared firing rates to the preferred stimulus class between sides for all stimulus-selective units that distinguished color images from gratings, i.e., all ‚Color' units from the preceding analysis ($n = 68$, crows pooled). We split the population of selective units into a group of color-preferring units ($FR_C > FR_{MS}$, $n = 48$) and a group of grating-preferring units ($FR_{MS} > FR_C$, $n = 20$) and calculated side indices for each unit, separately for both groups and all side combinations. Side indices SI were calculated with the formula $SI_{AB} = (FR_A - FR_B)/(FR_A + FR_B)$, where FR is the average firing rate to the preferred stimulus (image, static grating, or moving grating) and A and B are the sides being compared. Indices above or below zero indicate stronger responses to the preferred stimulus on one of the sides. Figure 3*A* shows the distribution of side indices for both groups and all comparisons. For grating-preferring units (*bottom row*), activity to the preferred stimulus on average did not differ between sides (average SI not different from zero, $P > 0.05$, *t* test). By contrast, color-preferring units (*top row*) showed increased activity to the preferred stimulus for right over left and for frontal over left stimuli [$SI_{LR} < 0$, $P < 0.001$, Wilcoxon signed-rank test; $SI_{LF} < 0$, $t(47) = -6.15$, $P < 0.001$, *t* test] with no difference between right and frontal stimuli [$t(47) = 1.49$, $P = 0.14$, *t* test]. Overall, units preferring color images showed increased activity for the contralateral hemifield.

We further analyzed the interaction of stimulus side and class. Of all recorded units, 32% in *crow 1* (58 of 181) and 22% in *crow 2* (46 of 209) showed a significant interaction (Supplemental Fig. S2, *E*–*G*). The exemplary units shown in Fig. 3, *B* and *C* selectively responded to color images in front or in front and on the right, but did not respond to gratings on any side. Across interaction units, stimulus class was mostly encoded for frontal and right but not left stimuli: a simple-effect analysis showed that significant proportions of interaction units distinguished color images from either type of grating in front (36 of 104, $P < 0.001$, Binomial test) and on the right (60 of 104, $P < 0.001$, Binomial test), whereas the majority of units did not distinguish stimulus classes on the left (Fig. 3*D*). In sum, interactions of side and stimulus resulted in selective stimulus coding for contralateral inputs, whereas stimulus class was not encoded for monocular ipsilateral inputs.

Tuning to Visual Features of Sine-Wave Gratings

We investigated whether left NCL units showed selective responses to controlled features of both static and moving sine-wave gratings. We determined feature-selective units with a multivariate sliding-window ANOVA for the factors side, spatial frequency, edge orientation, and, for moving gratings, motion direction ($P < 0.05$ for at least 11 consecutive time bins of 10 ms). The proportions of selective units for all factors and factor interactions in both crows are given in Table 1 for static gratings and Table 2 for moving gratings.

Static Gratings

We first analyzed responses to static gratings (Fig. 4). Around one-third of all units again showed side-selective responses irrespective of other features of static-grating stimuli (*crow 1*: 50 of 181 units; *crow 2*: 74 of 209 units). At the same time, around 11% of all units responded selectively to different spatial frequency levels (*crow 1*: 31 of 181 units; *crow 2*: 12 of 209 units). An example of a frequency-selective unit is shown in Fig. 4*A*. We compared the preferred frequency eliciting highest FRs across all selective units pooled between crows. Most frequency-selective units preferred high spatial frequencies with a peak at 2 cycles/°, followed by the lowest frequency tested at 0.08 cycles/° (Fig. 4*B*). By contrast, only few units showed selective responses to edge orientation (*crow 1*: 19 of 181 units; *crow 2*: 6 of 209 units).

We next investigated whether feature-selective responses to static gratings were modulated by stimulus position. Several units showed a significant interaction of stimulus side and spatial frequency (Fig. 4*C*) or of side and edge orientation (Fig. 4*D*). To test whether spatial frequency was better differentiated at specific positions in the visual field, we compared average FRs between frequency levels separately for each side. Per side, we applied a Kruskal–Wallis test for the factor spatial frequency to all recorded units in a fixed 500-ms time window, starting 150 ms after stimulus onset.

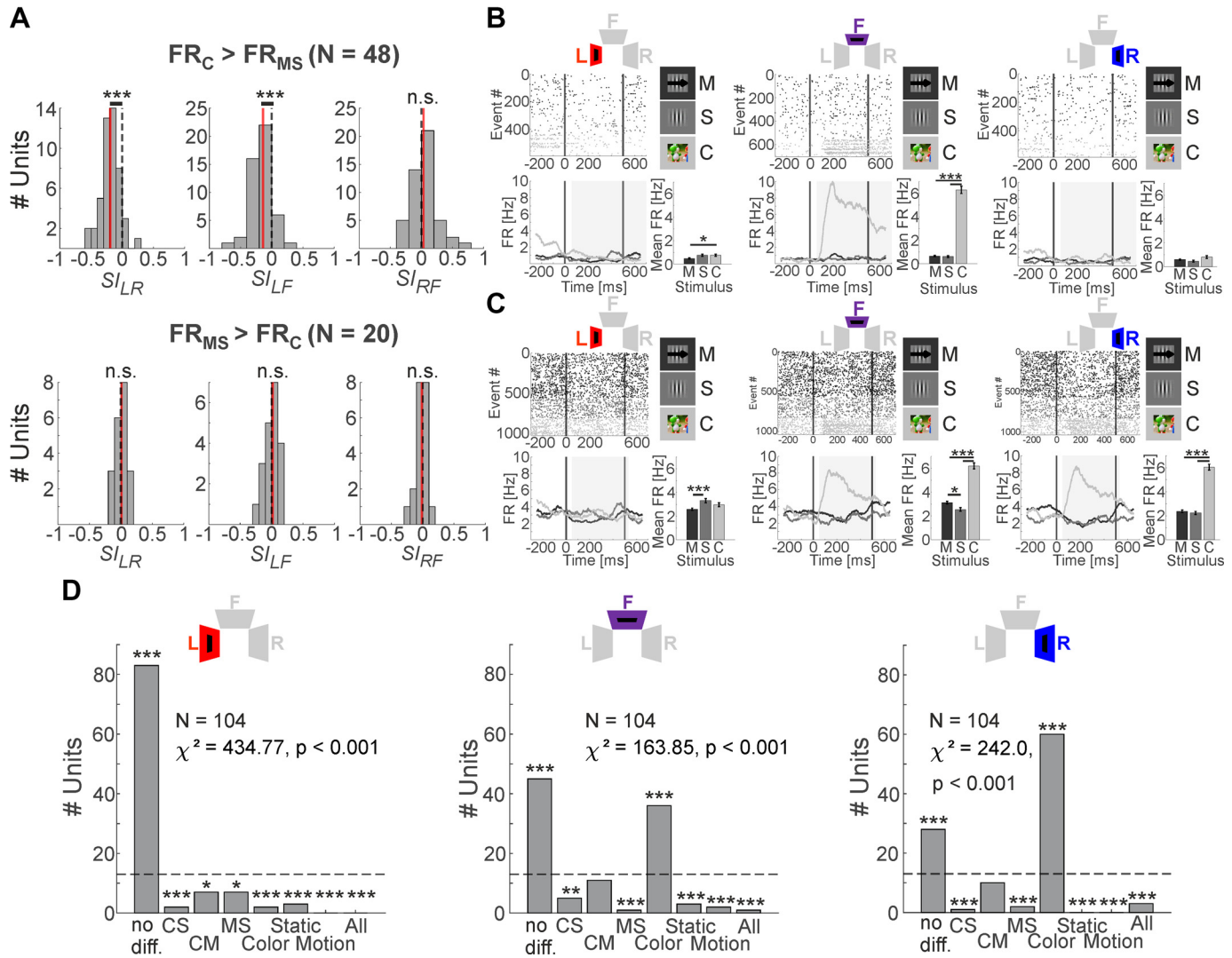

Figure 3. Interaction of stimulus position and class. *A*: distribution of side indices calculated from responses to preferred stimuli for selective units preferring color images over gratings ($N = 48$, *top row*) or preferring gratings over images ($N = 20$, *bottom row*). Activity is compared between left and right stimuli (*left column*), left and front stimuli (*middle column*) and right and front stimuli (*right column*). $^{***}P < 0.001$, *t* test/Wilcoxon signed-rank test. Activity of an exemplary interaction unit in *crow 1* (*B*) and *crow 2* (C). Shown are the responses to stimulus class separately for the left (*left column*), front (*middle column*), and right position (*right column*). *D*: simple-effect analysis of interaction units ($N = 104$, Crows pooled). For each side, average firing rates (FRs) to different stimulus classes were compared using pairwise post hoc comparisons (unpaired *t* test, Bonferroni corrected). Per side, units were then sorted by response profile. Although most units did not encode stimulus class for left stimuli ("no diff."), a significant subpopulation distinguished color images from either grating type for front and right stimuli ("Color"). The dashed lines indicate the number of units per profile expected from a uniform distribution. $^{*}P < 0.05$, $^{**}P < 0.01$, $^{***}P < 0.001$, Binomial test against chance. CM, significant difference only between color and motion; CS, significant difference only between color and static; MS, significant difference only between motion and static.

Figure 4*E* shows the relative proportions of frequency-selective units per side in both crows. Notably, most selective responses in *crow 1*, around 15% of all recorded units, were confined to right-monocular stimuli ($n = 50$ of 181, $P < 0.001$, χ^2 test of number of units per side). However, there was no difference between sides in the number of frequency-selective units in *crow 2* ($n = 40$ of 209, $P = 0.2$, χ^2 test). Similar results were found for the distribution of orientation-selective responses per side (Fig. 4*F*): *crow 1* showed a higher proportion of selective responses for frontal and right stimuli than for left stimuli ($n = 34$ of 181, $P = 0.015$, χ^2 test), whereas there was no difference between sides for *crow 2* ($n = 33$ of 209, $P = 0.42$, χ^2 test). In sum, only small proportions of left NCL units showed frequency- or orientation-selective responses with an overall preference for higher frequencies. Feature-selective responses were more prominent in the contralateral half-field in *crow 1*.

Moving Gratings

We next investigated selective responses to moving gratings with the additional factor of motion direction (Fig. 5). Almost half of all units showed side-selective responses irrespective of other features (*crow 1*: 72 of 181 units; *crow 2*: 96 of 209 units), a slightly higher proportion than for static gratings. Across crows, moving gratings elicited the same amount of spatial-frequency-selective responses as static gratings at 11% of all units (*crow 1*: 27 of 181 units; *crow 2*: 16 of 209 units). A frequency-selective unit is shown in Fig. 5*A*.

Table 1. *Feature-selective units for static gratings*

	Factor	*Crow 1*	*Crow 2*
Main effect	Side	50/181 (28%)	74/209 (35%)
	Frequency	31/181 (17%)	12/209 (6%)
	Orientation	19/181 (11%)	6/209 (3%)
Two-way interaction	Side × Frequency	29/181 (16%)	19/209 (9%)
	Side × Orientation	10/181 (6%)	19/209 (9%)
	Frequency × Orientation	25/181 (14%)	18/209 (9%)
Three-way interaction	Side × Frequency × Orientation	26/181 (14%)	24/209 (12%)

The absolute and relative proportion of selective units as assessed by a sliding-window ANOVA is given for both subjects for all main effects and interactions. Units with P values below 0.05 for at least 11 consecutive 10-ms time bins were considered selective, starting 50 ms or later after stimulus onset.

Notably, only 5 units showed frequency selectivity for both static and moving gratings, indicating that stationary and moving stimuli activated distinct subpopulations. Again, we examined the distribution of preferred frequencies for selective units pooled between crows (Fig. 5*B*). Comparable with static gratings, frequency-selective units overall preferred higher frequencies with a peak at 2 cycles/°. Orientation-selective responses were also comparable with static gratings with only a low number of selective units (*crow 1*: 7 of 181 units; *crow 2*: 16 of 209 units). Notably, the additional parameter of motion direction did not elicit a higher number of selective responses: direction-selective units between crows were comparable in number to orientation-selective units (*crow 1*: 21 of 181 units; *crow 2*: 6 of 209 units). As for static gratings, we next analyzed interactions with stimulus side. Overall, a similar proportion of units as for static gratings showed significant interactions of side and spatial frequency (Fig. 5*C*) and of side and edge orientation. A low number of units showed an interaction of side and motion direction (*crow 1*: 14 of 181 units; *crow 2*: 13 of 209 units) (Fig. 5*D*). We assessed feature-selective responses per side using separate Kruskal–Wallis tests of spatial frequency and motion direction for all recorded units. Although both crows showed slightly higher proportions of frequency-selective responses to frontal and right than to left stimuli (Fig. 5*E*), this did not reach significance in either crow (*crow 1:* $n = 42$ of 181, $P = 0.58$; *crow 2:* $n = 28$ of 209, $P = 0.2$, χ^2 test of number of units per side). Similarly, there was no side difference in the proportion of direction-selective responses (Fig. 5*F*) (*crow 1:* $n = 32$ of 181, $P = 0.79$; *crow 2:* $n = 27$ of 209, $P = 0.71$, χ^2 test). Overall, moving sine-wave gratings elicited responses similar to static gratings. A small number of units in addition showed interactions between side and motion direction, but this interaction was not consistent across units.

An additional analysis of direction selectivity using circular statistics confirmed these results. We tested the directional responses of all units against a uniform circular distribution ($P < 0.05$, Rayleigh test). In *crow 1*, only 3 of 181 units (1.7%) were direction-selective. In *crow 2*, only 2 of 209 units (1%) were direction-selective. A repetition of this analysis separately for each side revealed no difference between sides in the proportion of direction-selective units. *Crow 1* showed 1.7% selective responses on the left (3 of 181), 3.9% in front (7 of 181), and 2.2% on the right (4 of 181). For *crow 2*, there were 1.9% selective responses on the left (4 of 209), 1.9% in front (4 of 209), and 1.4% on the right (3 of 209). The proportion of selective units did not differ between sides (*crow 1:* $n = 14$ of 181, $P = 0.33$; *crow 2:* $n = 11$ of /209, $P = 0.91$, χ^2 test of number of units per side). In sum, there was no consistent direction selectivity in either crow.

Encoding of Complex Images across the Visual Fields

Besides gratings, we also presented a set of 18 color images (Supplemental Fig. S1) across all stimulus positions to assess responses to more complex stimuli (Fig. 6). We applied a two-way sliding-window ANOVA to all recorded units to analyze the factors side (left, front, right) and image (labeled 1–18). Figure 6*A* shows an example of an image-selective unit. These units typically showed increased FRs for a small subset of images. Overall, almost a third of all units showed side-selective responses in both crows, and a similar proportion showed image-selective responses (Fig. 6*B*). Across crows, color images strongly evoked selective activity with around half of all recorded units showing a significant main

Table 2. *Feature-selective units for moving gratings*

	Factor	*Crow 1*	*Crow 2*
Main effect	Side	72/181 (40%)	96/209 (46%)
	Frequency	27/181 (15%)	16/209 (8%)
	Direction	21/181 (12%)	6/209 (3%)
	Orientation	7/181 (4%)	16/209 (8%)
Two-way interaction	Side × Frequency	21/181 (12%)	17/209 (8%)
	Side × Direction	14/181 (8%)	13/209 (6%)
	Side × Orientation	15/181 (8%)	9/209 (4%)
	Frequency × Direction	23/181 (13%)	21/209 (10%)
	Frequency × Orientation	14/181 (8%)	11/209 (5%)
Three-way interaction	Side × Frequency × Direction	22/181 (12%)	24/209 (12%)
	Side × Frequency × Orientation	20/181 (11%)	14/209 (7%)

Conventions as in Table 1. The factor Direction was nested inside the factor Orientation, so no interactions between these factors were calculated.

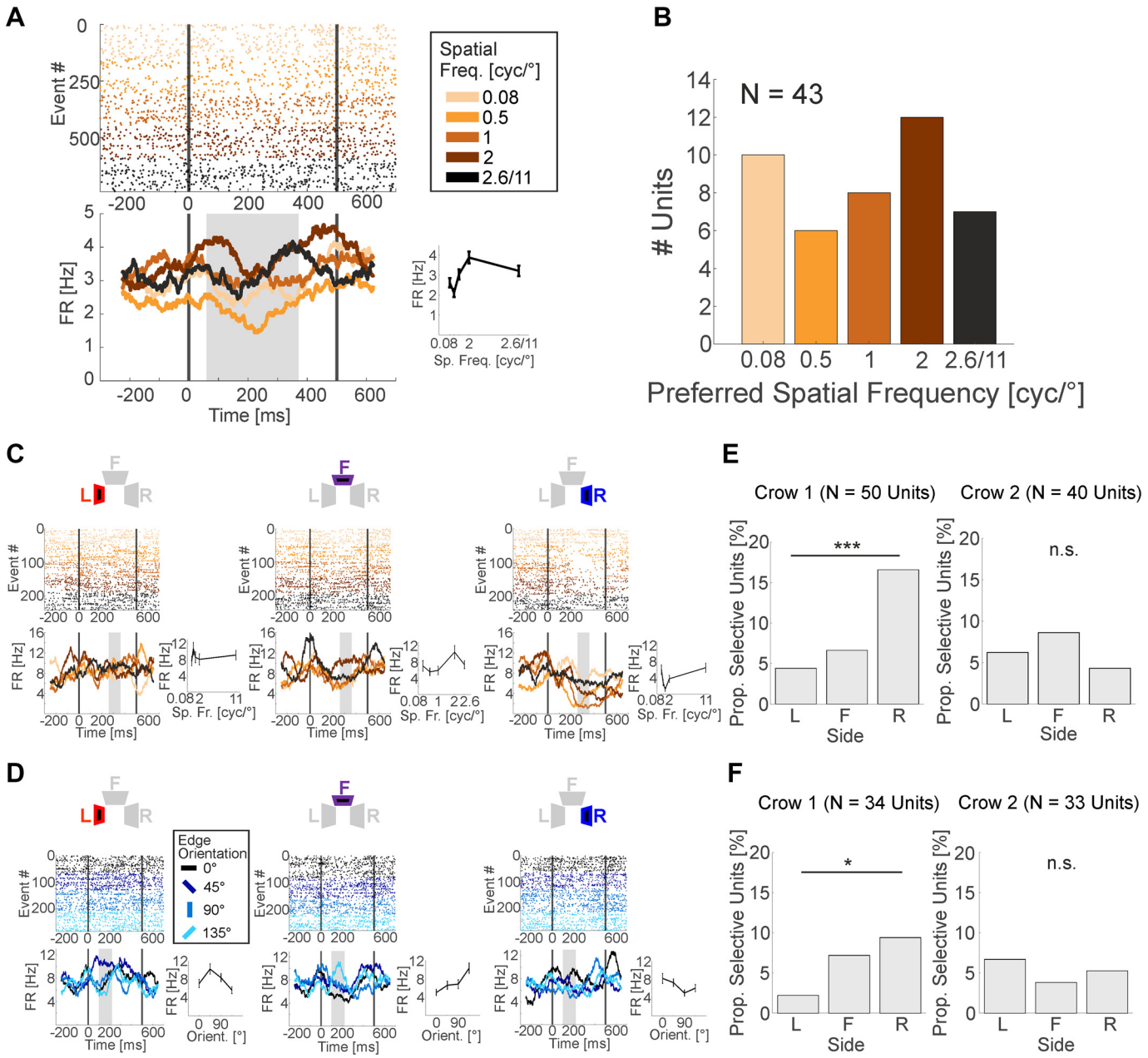

Figure 4. Tuning properties of nidopallium caudolaterale (NCL) units in response to static gratings. *A*: activity of an exemplary unit tuned to spatial frequency in *crow 1*. *Bottom right*: average firing rate (FR) across spatial frequencies in the selective time window. *B*: population tuning of frequency-selective units, *N* = number of selective units (sliding-window ANOVA). Shown are the numbers of units with highest FRs at the respective frequency. Most units preferred static gratings of 2 cycles/°. *C*: example unit showing an interaction of side and spatial frequency in *crow 1*. The response to different spatial frequencies is shown separately for left, front, and right stimuli. Selective frequency tuning was present for front and right but not left stimuli, and the preferred frequency differed between front and right stimuli. *D*: example unit showing an interaction of side and edge orientation in *crow 1*. Across sides, activity was highest for different orientations. *E*: proportion of spatial-frequency-tuned units across sides, *N* = number of selective units. For both crows, units were tested for selective frequency tuning separately for each side (Kruskal–Wallis test, $P < 0.05$). Shown is the relative proportion of selective units out of all units recorded. ***$P < 0.001$, χ^2 test. *F*: proportion of orientation-tuned units across sides. Conventions as in *E*. *$P < 0.05$, χ^2 test.

effect and/or an interaction. Because the two crows showed comparable results, we pooled selective units for further analysis. Our set of color images was not selected based on specific image contents, so we did not expect the population of selective units to be biased toward individual images. To assess if image-selective responses were biased to specific images across units, we sorted all image-selective units by their preferred image, evoking the highest average FR (Fig. 6*C*). The resulting distribution did not differ from a uniform distribution ($n = 104$, $\chi^2 = 26.5$, $P = 0.066$), indicating that selective responses across units were not biased toward specific image contents.

Next, we analyzed if image-selective responses interacted with stimulus side. Of all recorded units, 29% in *crow 1* and 17% in *crow 2* showed a significant interaction of image and side. An exemplary interaction unit is shown in Fig. 6*D*. This

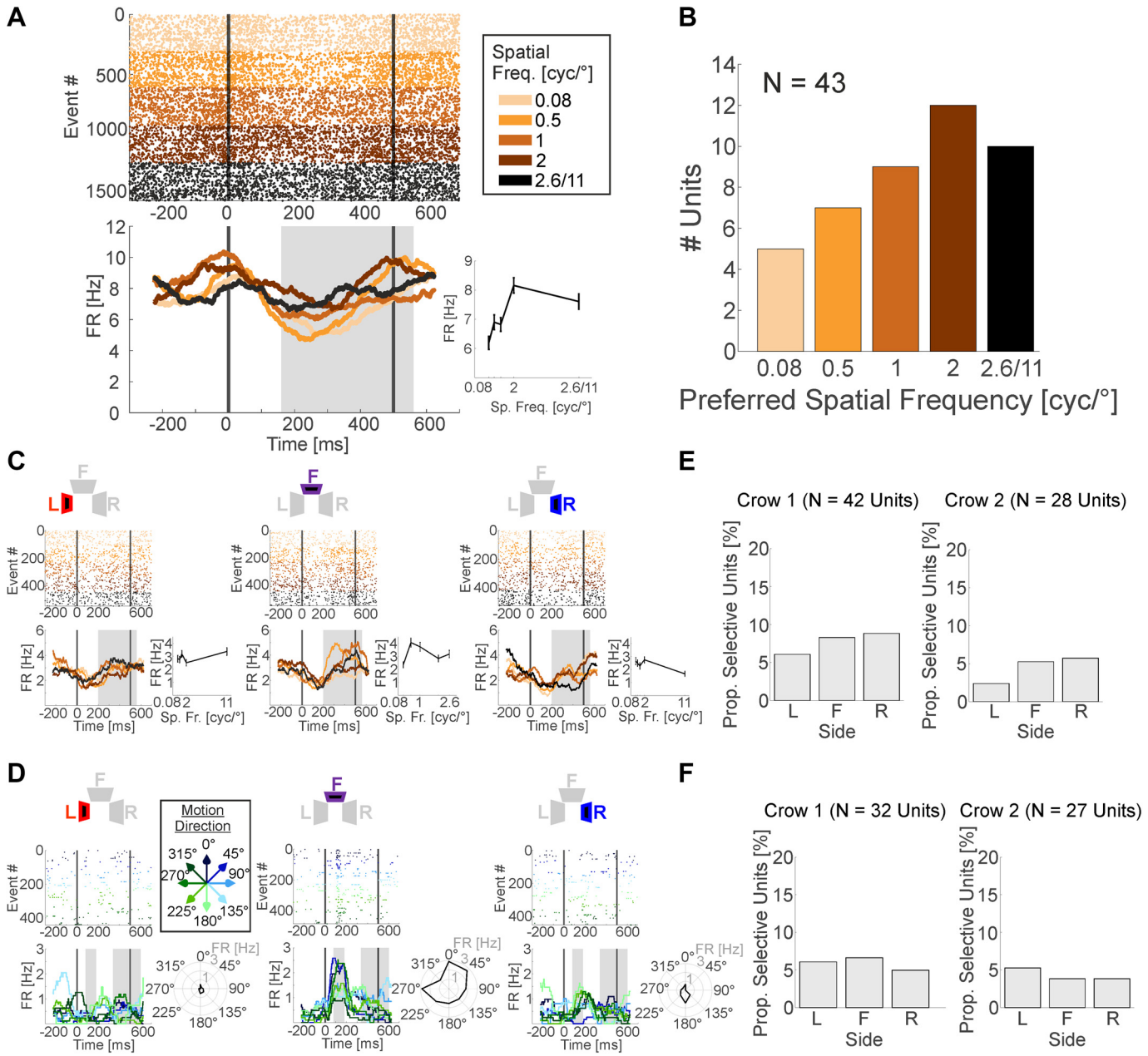

Figure 5. Tuning properties of nidopallium caudolaterale (NCL) units in response to moving gratings. *A*: activity of an exemplary unit tuned to spatial frequency in *crow 1*. *B*: population tuning of frequency-selective units. Most units preferred moving gratings of 2 cycles/°. *N* = number of selective units (sliding-window ANOVA). *C*: example unit showing an interaction of side and spatial frequency in *crow 2*. Activity increased for intermediate frequencies of front but not side stimuli. *D*: example unit showing an interaction of side and motion direction in *crow 2*. Gray shading indicates two separate time windows with significant interactions. Polar plots indicate the average directional tuning per side in the first interaction window. The radial axis indicates firing rates (FRs). *E*: proportion of spatial-frequency-tuned units across sides for both crows. *F*: proportion of motion-direction-tuned units across sides for both crows, *N* = number of selective units (Kruskal–Wallis test per side, $P < 0.05$).

unit significantly increased FR for a subset of images, but only when they appeared in front or on the right. Its preferred image was the same for both positions. To analyze if interactions systematically modulated FRs between sides, we calculated side indices for image-selective units ($n = 104$) and compared FRs to the preferred image between all pairs of side (Fig. 6*E*). Across image-selective units, the preferred image evoked higher FRs for right than for left stimuli ($SI_{LR} < 0$, $P < 0.001$, Wilcoxon signed-rank test) and for frontal than for left stimuli [$SI_{LF} < 0$, $t(103) = -4.1$, $P < 0.001$, t test]. By contrast, there was no difference between right and frontal stimuli [$t(103) = 0.06$, $P = 0.95$, t test].

Next, we split image-selective units in two groups: units that additionally showed an interaction of image and side ($n = 53$ of 104), and units with no interaction ($n = 51$ of 104). We then compared the distribution of side indices between groups to determine whether interactions drove the bias in image-selective responses. Groups did not differ in left-right indices (int.: $SI_{LR} = -0.29$, no int.: $SI_{LR} = -0.19$, $P = 0.19$,

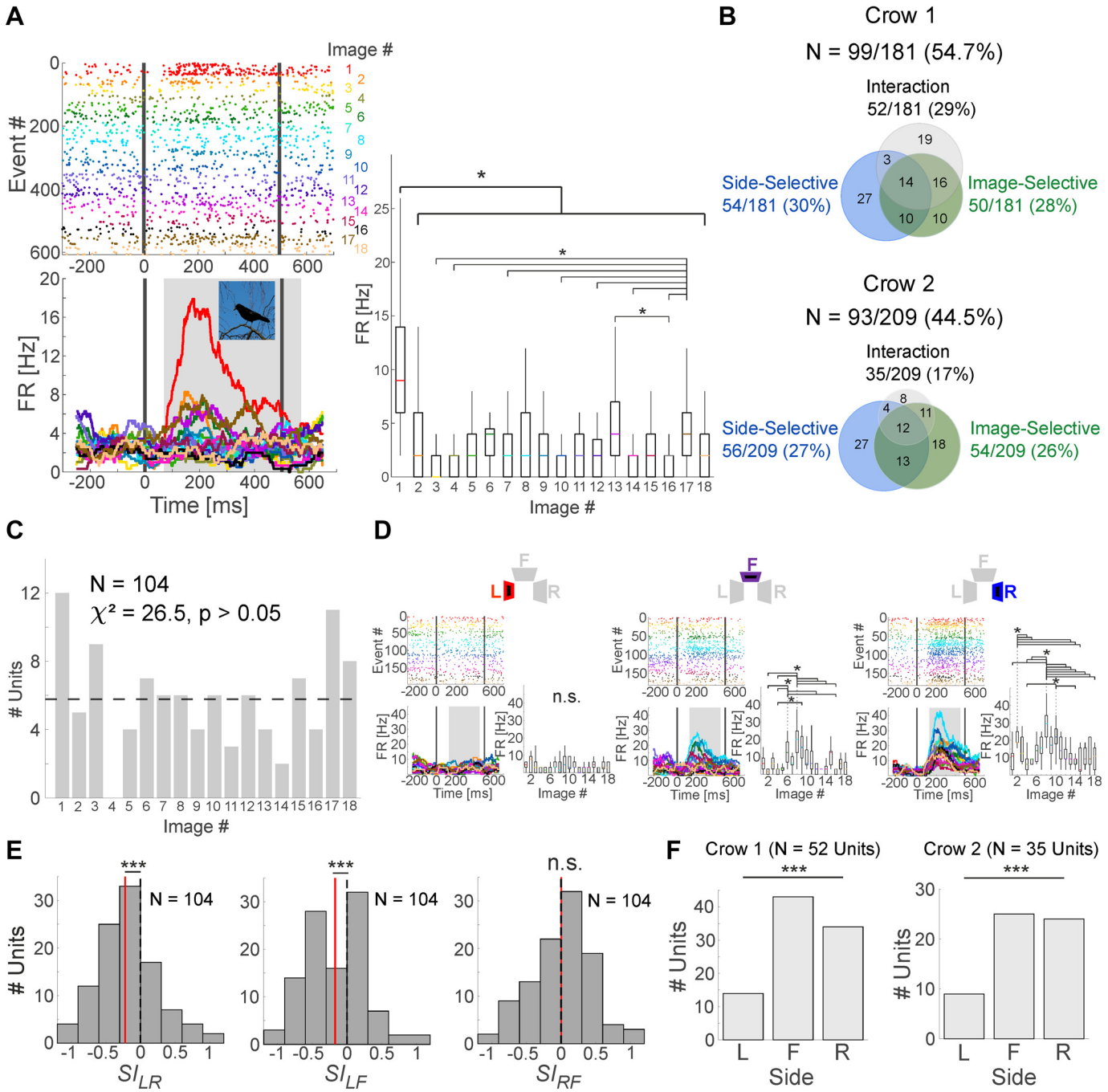

Figure 6. Tuning properties of nidopallium caudolaterale (NCL) units in response to color images. *A*: activity of an exemplary image-selective unit in *crow 2*. Stimuli are grouped by image and color-coded according to image labels. *Left*: stimulus response over time aligned by stimulus on- and offset (black lines). Gray shading indicates the time window of selective image responses. Firing rates (FRs) increased in response to the inset picture. *Right*: average tuning across images in selective time window. Colored lines indicate median FR per image. *Image 1* elicited consistently higher activity compared with all other images. $*P < 0.05$, unpaired *t* test, Bonferroni corrected. *B*: proportion of side-selective, image-selective and interaction units in *crow 1* (*top*) and *crow 2* (*bottom*). *N* = number of selective units among all analyzed units (sliding-window ANOVA). *C*: population tuning of image-selective units (Crows pooled). Shown is the number of units with highest average FR per image. Image preferences did not differ from a uniform distribution (dashed line, χ^2 test). *D*: example unit showing an interaction of side and image in *crow 1*. The unit showed an image-selective increase in FR for front and right but not left stimuli. The preferred image was the same for front and right stimuli. *E*: distribution of side indices, calculated from responses to preferred images for image-selective units ($N = 104$, Crows pooled). Activity is compared between left and right stimuli (*left*), left and front stimuli (*middle*), and right and front stimuli (*right*). $***P < 0.001$, Wilcoxon signed-rank test/*t* test. *F*: simple-effect analysis of interaction units for both crows. Per side, interaction units were tested for image-selective responses (Kruskal–Wallis test, $P < 0.05$). $***P < 0.001$, χ^2 test.

Mann–Whitney U test), so the increased response to right over left preferred stimuli was independent of the presence of an overall interaction. By contrast, interactions led to more negative left-front indices (int.: $SI_{LF} = -0.37$, no int.: $SI_{LF} = 0.07$, $P < 0.001$, Mann–Whitney U test) and more negative right-front indices (int.: $SI_{RF} = -0.11$, no int.: $SI_{RF} = 0.13$, $P = 0.034$, Mann–Whitney U test). Thus, interaction units showed stronger tuning to the preferred image when it was shown in the frontal, binocular field compared with either monocular field.

Finally, we performed a simple-effect analysis of all interaction units, irrespective of the main effect of image or side. For this, we applied a Kruskal-Wallis test for the factor image separately for each side. Figure 6*F* shows the number of interaction units with significant image selectivity per side. In both crows, most units showed image-selective responses for frontal and right stimuli (*crow 1*: 52 of 181, $P < 0.001$; *crow 2*: 35 of 209, $P < 0.001$, χ^2 test of number of units per side). Taken together, complex images strongly evoked selective activity with most pronounced tuning to preferred images in the contralateral half-field, leading to a consistent interaction of image content and stimulus position across units.

Stable Population Coding of Stimulus Position and Class across the Visual Field

We investigated whether the population activity of recorded NCL units carried consistent information about stimulus side and class. For this, we trained and tested a multiclass support-vector machine (SVM) on the average responses of all recorded units ($n = 390$, crows pooled) to all 234 stimuli (Fig. 7). We determined classification accuracy using sixfold cross-validation for both side and class and compared our model to a random SVM trained and tested with shuffled class labels (1,000 redraws). Stimulus side was decoded with near-perfect accuracy above 90% for all sides with no notable confusion (Fig. 7*A*). The model performed significantly better than chance for all sides (Fig. 7*B*). This confirms that left-NCL activity is modulated by stimulus side, distinguishing between ipsilateral monocular, contralateral monocular, and frontal binocular input.

We next trained an SVM model to decode stimulus class with the same approach, irrespective of stimulus side. The classifier correctly decoded 88.3% of moving gratings and 74.1% of color images, whereas only 50% of static gratings were labeled correctly (Fig. 7*C*). Notably, any misclassified grating stimuli, static or moving, were confused with the other class of gratings, respectively, but never with color images. For static and moving gratings, the asymmetry in the confusion matrix suggests that the additional feature of motion induced characteristic activity patterns that reduced confusion with static gratings. Still, across all stimulus classes, our model performed significantly better than chance (Fig. 7*D*). This confirms that population activity encoded stimulus class in addition to side.

Finally, we investigated whether population coding of stimulus class was affected by stimulus side. We repeated our SVM analysis of stimulus class separately for each side, so we trained and tested separate models on the subsets of left, frontal, and right stimuli (Fig. 8). All other parameters were identical between sides and to the preceding analysis. Classification results were largely comparable across sides: Both gratings and color images were decoded significantly better than chance for left stimuli (Fig. 8, *A* and *B*), frontal stimuli (Fig. 8, *C* and *D*), and right stimuli (Fig. 8, *E* and *F*). These results were also comparable with the model trained on all sides (Fig. 7, *C* and *D*) because the most common confusion across models was static gratings being misclassified as moving gratings. For all classes, the highest accuracy was achieved for right stimuli. The biggest difference between sides was the lowered classification accuracy for color images on the left with 55.6%, compared with the front with 88.9%, and the right with 94.4%. This means that the front and the right model classified images more accurately than the model trained on all sides, whereas the left model was less accurate. Overall, this shows that population activity distinguished complex images better in the contralateral half-field than in the ipsilateral monocular field, whereas sine-wave gratings were encoded equally well across the visual fields.

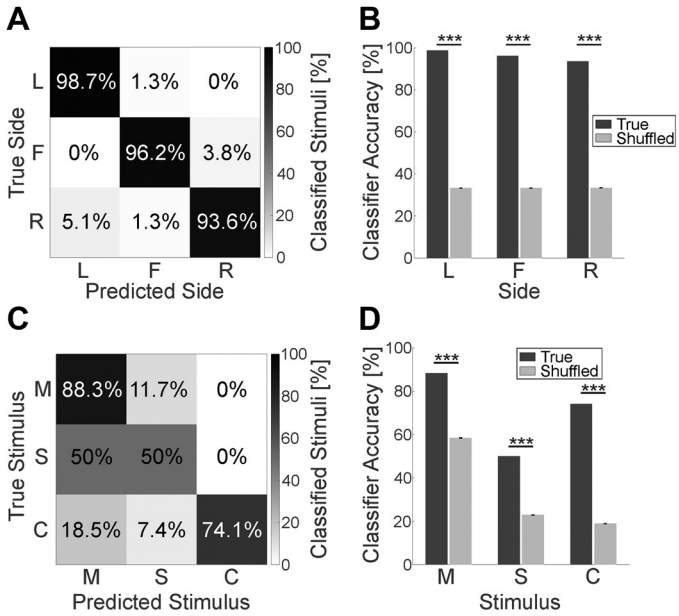

Figure 7. Nidopallium caudolaterale (NCL) population activity encodes both stimulus position and class. *A*: confusion matrix with classification results of a support-vector machine (SVM) trained to decode stimulus side from average population activity, pooled between crows. Rows indicate actual stimulus position, columns the position predicted by the classifier. Intensity indicates the proportion of classified stimuli per combination of true and predicted side. *B*: classification accuracy for stimulus side. Dark bars indicate accuracy per side of the model shown in *A*. Light bars indicate accuracy per side of a model trained and tested with randomly shuffled side labels, averaged across 1,000 runs. Error bars indicate the means ± SE. ***$P < 0.001$, Monte-Carlo P values. *C*: confusion matrix showing classification results of an SVM trained to decode stimulus class. Conventions as in *A*. *D*: classification accuracy for stimulus class. Conventions as in *B*. ***$P < 0.001$, Monte-Carlo P values.

DISCUSSION

Neural activity in the left NCL of awake crows was strongly influenced by stimulus position. Distinct subpopulations responded either to frontal binocular stimuli or to both frontal and contralateral monocular stimuli, i.e., to right-eye inputs. Single units responded to complex visual information with distinct preferences for specific images that were most pronounced for frontal and contralateral stimuli. By contrast, local parametric features of sine-wave gratings were not

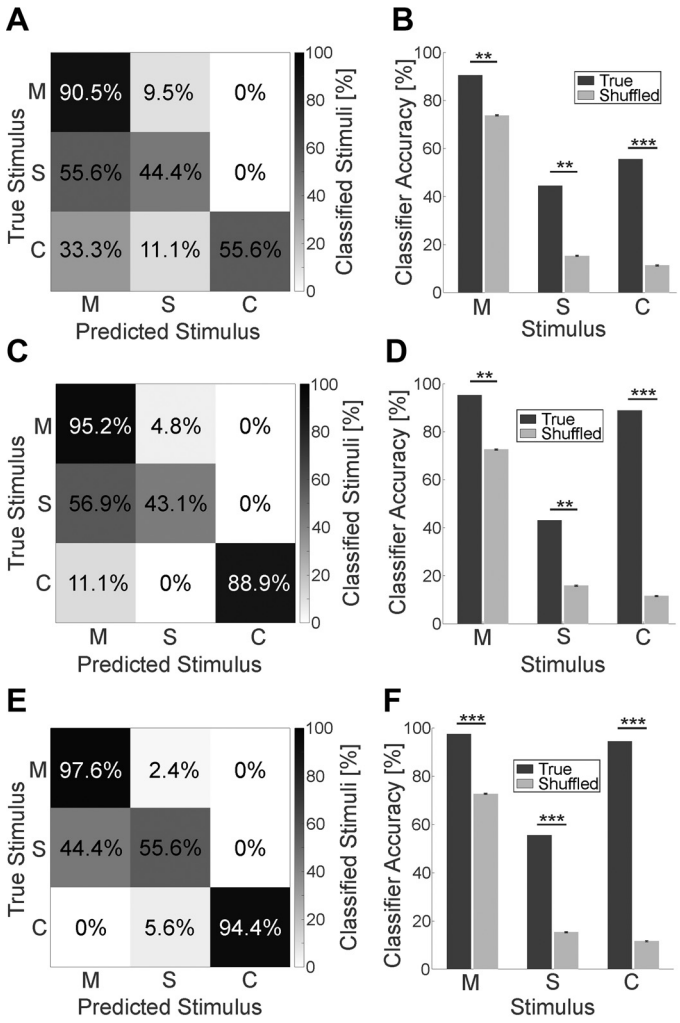

Figure 8. Population coding of stimulus class is preserved across sides. *A*: confusion matrix showing classification results of an support-vector machine (SVM) trained to decode stimulus class from average population activity to left stimuli, pooled between crows. *B*: classification accuracy for stimulus class of left stimuli. The model shown in *A* performed significantly better than a random model trained on shuffled labels. $^{**}P < 0.01$, $^{***}P < 0.001$, Monte-Carlo *P* values. Confusion matrix (*C*) and classification accuracy (*D*) for stimulus class of front stimuli. Conventions as in *A* and *B*. Confusion matrix (*E*) and classification accuracy (*F*) for stimulus class of right stimuli. Conventions as in *A* and *B*.

consistently encoded except for a general preference for high spatial frequencies. Population activity reliably encoded stimulus side and class, except between static and moving gratings. These findings indicate that left NCL integrates input from both eyes to represent different regions of the visual field.

Encoding of Stimulus Position

Previous studies have recorded NCL activity in crows responding to visual stimuli at varying spatial positions (35–37). These studies showed that single NCL units can dynamically represent the position of targets the crows had to actively peck at. Across studies, all tested positions were encoded during motor planning and execution, and there was no systematic difference between the left and right visual hemifields for either brain hemisphere. Importantly, all of these studies presented stimuli on a screen directly in front of the crows. Thus, NCL units could distinguish precise locations within the frontal visual field.

However, it remained unclear whether this spatial encoding would be restricted to frontal in contrast to lateral stimuli. Our results show that a relevant subpopulation of left NCL units responds in a dedicated manner to the frontal binocular field. Such units could encode precise visuospatial information about objects that are in pecking range. This is also supported by our finding that more than 20% of recorded units showed an interaction of position and image content for the color image set. These units were most strongly activated by their preferred image when it appeared in the binocular field. Moreover, a gaze-tracking study in large-billed crows recently showed that crows track moving objects using their binocular field even at a distance (49). Taken together, the current data on spatial coding in the crow NCL are thus in line with functional specializations of the optic system that support binocular frontal vision (44, 49, 50).

Previous crow studies did not test the left and right eyes separately. Instead, visual stimuli were always in the binocular field range. A recent study in pigeons recorded NCL activity bilaterally while the birds engaged in a visual go/no-go task (51). In that task, pure colors were presented to either the left or the right eye to investigate asymmetries of visual processing between left and right NCL. In agreement with our results, the authors found both task-related units responding only for one eye (monocular response) and units responding for either eye (binocular response). However, the stimulation protocol differed from our study in several ways: first, pigeons were only shown simple colors, whereas we presented both controlled sine-wave gratings and complex images, revealing a difference between simple local features and complex composed stimuli. Second, the color stimuli were shown to pigeons at a 5 cm distance from each eye. This prevents coactivation of the contralateral eye but precludes a distinction between different parts of the visual field within eyes. This is important because units like the one shown in Fig. 2*A* did not simply respond to any visual input, but specifically to a coactivation in the frontal field of both eyes. In fact, we determined neural selectivity by comparing FRs between the individual factor levels, rather than to an average activity baseline. For this reason, the observed response selectivities could result from opposite responses, i.e., excitatory versus inhibitory, to stimuli placed on different sides as shown in Fig. 2*B*. Therefore, left NCL seems to distinguish not only monocular and binocular stimuli, but specifically between inputs from different retinal areas.

Selectivity for Local versus Global Features

Neural responses to complex, colorful images were consistently different from responses to sine-wave gratings. This led to significant encoding of stimulus class on both the single-cell and population level. Notably, we found many units with selective responses to specific images. By contrast, only very few neurons showed selective tuning toward specific grating features such as edge orientation or motion direction. Moreover, static and moving gratings elicited mostly comparable responses. This is surprising because NCL receives direct input from visual areas known to encode local stimulus features: tectofugal input comes from the caudal

entopallium that has been shown to encode motion information on the single-cell level (52) and is important for motion perception (53). Thalamofugal input comes from the visual hyperpallium that has been likened to mammalian V1 (3). In owls, this area encodes various parametric features on the single-cell level, including orientation, motion direction, temporal and spatial frequency, and binocular disparity (10, 14, 15, 54). When owls passively viewed plaid stimuli composed of overlaid moving gratings, hyperpallial cells selectively encoded local but not global motion direction (10). In the crow NCL, neural encoding of motion direction has been shown for moving dot patterns in a working memory task (38), suggesting that motion integration may occur only at this processing stage. However, comparisons across studies are complicated by the fact that owls are heavily specialized birds of prey. Their hyperpallium is hypertrophied relative to brain volume (55) and overrepresents the frontal binocular field, reflective of their frontally shifted eye position (56). Moreover, the dot patterns shown to the crows had 100% motion coherence, so local motion information could not be distinguished from global motion. Even so, 28% of neurons were direction-selective in the active task, whereas we found fewer than 10% in our passive task, suggesting that stimulus complexity may account for the discrepancy.

An alternative explanation for this result is that NCL dynamically recruits motion information when it becomes task-relevant. In our protocol, crows had to withhold orienting responses to the stimuli and did not need to distinguish different feature levels. Dynamic coding in associative areas has been suggested to rely on flexible recruitment of neuronal ensembles, depending on behavioral context (4). Comparable with the mammalian prefrontal cortex, NCL also integrates dopaminergic input from the midbrain that contributes to executive functioning and reward learning (57, 58). Similarly, allocating attention to visual stimuli modulates the response properties of prefrontal neurons (59). Moreover, NCL directly projects into the premotor arcopallium (29) and is involved in motor planning (37, 42, 60). The absence of goal-directed action initiation in our task may thus explain the low number of feature-selective responses.

In contrast to monochrome gratings, a much higher proportion of units showed selective activity for specific color images. This difference between stimulus classes could be a result of the relative frequency of each class: moving and static gratings comprised 77% of our stimulus set due to the higher number of unique feature combinations. Color images made up the remaining 23% of stimuli and thus appeared much less frequently. Although we did not directly control for stimulus frequency, previous recordings in pigeons show that NCL activity may be affected by the level of informational surprise conveyed by task events: Packheiser et al. (61) found that NCL single-unit activity was associated with reward prediction errors, signaling a discrepancy between expected and observed outcome. Crows have been shown to extract statistical information from arbitrary stimuli (62), so the relative frequencies of gratings versus color images in our protocol could have affected NCL activity in the awake crows. However, more direct investigations of surprise coding in NCL are needed to draw definite conclusions.

Although motion and orientation were not consistently encoded by single units, we found around 10% of units with selective responses to spatial frequencies. Most units preferred static or moving gratings with higher spatial frequencies, with a peak around 2 cycles/°. The range of frequencies we could test was limited by our setup's combination of screen resolution and viewing distance. Still, our maximal frequencies of 2.6 and 11 cycles/° fell in the order of magnitude previously reported for maximal visual acuity in crows (63). Because we presented moving gratings at a constant velocity of 16°/s, temporal frequency (measured in cycles/s) always covaried with spatial frequency. Thus, selective responses to moving gratings in our task could have resulted from temporal rather than spatial frequency coding, or from a mixture of both. Such spatiotemporal tuning has been shown in the visual hyperpallium in owls (54). Although we cannot entirely exclude this possibility, the population tuning to moving gratings was comparable with the static gratings that varied only in spatial frequency. Therefore, we suggest that selective NCL units are preferentially tuned to high spatial frequencies. This would be consistent with behavioral measurements of visual acuity.

Compared with other songbirds, corvids overall achieve higher visual acuities than expected by eye size alone (64). Such a positive correlation between population tuning and acuity is also present in the striate cortex of mammals for spatial but not for temporal frequency (65). In the case of corvids, this result may reflect an adaptation to their generalist lifestyle (66). Selective tuning of NCL units toward high spatial frequencies across the visual field may thus support flexible behavior in response to a dynamic visual environment.

Interaction of Stimulus Position and Content

Across several analyses, neural responses to identical stimulus features varied between different positions in the visual field. Color-preferring units responded strongest to frontal and right images. In addition, interactions between position and stimulus class revealed consistent differentiation of color images versus gratings at these positions, but not for left stimuli. In turn, different color images evoked selective responses that were stronger for frontal and right than for left stimuli. Interactions between side and image revealed that selective responses to specific images were more common in front and on the right than on the left. And finally, selective encoding of frequency and orientation of static gratings was more common in front and on the right in *crow 1*. Taken together, these results show that the left NCL encodes stimulus features more precisely for contralateral right-eye inputs than for ipsilateral monocular inputs.

This finding is consistent with the high degree of contralateral processing in the avian visual system. In birds, information from the whole retina crosses over to the contralateral hemisphere at the optic chiasm. The majority of fibers is then fed into the tectofugal pathway starting at the optic tectum (13). The optic tectum then projects to the nucleus rotundus of both hemispheres, but most projections are ipsilateral, maintaining a dominantly contralateral mapping of the visual field (23). Similarly, the lateral geniculate nucleus p. dorsalis (GLd) processes fully contralateral information and projects mostly to the ipsilateral hyperpallium, although some GLd components project bilaterally (67). Thus, both the tectofugal and thalamofugal stream that converge in NCL likely provide more detailed information about the contralateral hemifield.

It should be noted, however, that our recorded units were not unresponsive to left monocular stimuli in general. For instance, around 18% of all units encoded stimulus class independent of position, thus including left stimuli. This may also explain why our SVM classifier decoded stimulus class above chance level for all positions. At the same time, decoding accuracy was worst for left stimuli, and this was most notable for the image class. Thus, the classifier confused images with gratings much more often on the left. In sum, it seems that left NCL does integrate some information about the ipsilateral visual field from the ipsilateral eye, although less precisely than for frontal and contralateral inputs. This is reminiscent of responses to ipsilateral stimulation in the visual hyperpallium of zebra finches (16).

Asymmetry of Visual Processing

Electrophysiological studies with bilateral penetrations in pigeons and chicks have revealed functional asymmetries between left and right equivalent areas along the tectofugal pathway (19). A higher degree of bilateral integration has now been demonstrated for the left-hemispheric entopallium (24, 68) and NCL (51). In pigeons, this asymmetry is based on the larger number of contralateral tectal projections to the left Rt (23). These results support the view that commissural asymmetries of the tecto-rotundal projection lead to a more complete representation of the field of view across both eyes in the left hemisphere (26). The left hemisphere may then take control over visually guided behavior like discrimination and response selection (51).

Our results on the left NCL in crows are consistent with an integrated representation of the visual environment in the left hemisphere of the avian brain. However, because we did not investigate the right NCL activity in the same protocol, it remains unclear whether crows show a similar asymmetry of visual processing. Given that both anatomical and temporal patterns of lateralization differ between pigeons and chickens (69), caution must be taken when comparing species from different phylogenetic groups. Crows belong to the larger clade of oscine songbirds, for which the best-studied case of brain asymmetry is the song system (19). However, much less is known about asymmetries of the visual system in songbirds. In crows, we recently found behavioral evidence for an asymmetry of volitional visual attention (70). This suggests an asymmetry of higher visual processing in the crow brain. Combining bilateral brain recordings with active behavioral protocols should uncover the neural underpinnings of lateralized vision in crows.

ETHICAL APPROVALS

All procedures were carried out according to the guidelines for animal experimentation and approved by the responsible authorities under national legislation, the Regierungspräsidium Tübingen, Germany.

DATA AVAILABILITY

The data supporting the findings of this study are available from the corresponding author upon reasonable request.

SUPPLEMENTAL MATERIAL

Supplemental Figs. S1–S3: https://doi.org/10.6084/m9.figshare.30128662.

ACKNOWLEDGMENTS

We thank Julian Rühle for technical support.

GRANTS

This research was supported by Grant NI 618/12-1 (to A.N.) by the Deutsche Forschungsgemeinschaft (DFG) (German Research Foundation).

DISCLOSURES

No conflicts of interest, financial or otherwise, are declared by the authors.

AUTHOR CONTRIBUTIONS

L. Hahner and A.N. conceived and designed research; L. Hahner and L. Hoeppe performed experiments; L. Hahner, L. Hoeppe, and A.N. analyzed data; L. Hahner, L. Hoeppe, and A.N. interpreted results of experiments; L. Hahner prepared figures; L. Hahner and A.N. drafted manuscript; L. Hahner and A.N. edited and revised manuscript; L. Hahner, L. Hoeppe, and A.N. approved final version of manuscript.

REFERENCES

1. **Hall WC.** Visual pathways to the telencephalon in reptiles and mammals. *Brain Behav Evol* 5: 95–113, 1972. doi:10.1159/000123741.
2. **Van Essen DC**, **Maunsell JHR.** Hierarchical organization and functional streams in the visual cortex. *Trends Neurosci* 6: 370–375, 1983. doi:10.1016/0166-2236(83)90167-4.
3. **Knudsen EI.** Evolution of neural processing for visual perception in vertebrates. *J Comp Neurol* 528: 2888–2901, 2020. doi:10.1002/cne.24871.
4. **Hanganu-Opatz IL**, **Klausberger T**, **Sigurdsson T**, **Nieder A**, **Jacob SN**, **Bartos M**, **Sauer JF**, **Durstewitz D**, **Leibold C**, **Diester I.** Resolving the prefrontal mechanisms of adaptive cognitive behaviors: a cross-species perspective. *Neuron* 111: 1020–1036, 2023. doi:10.1016/j.neuron.2023.03.017.
5. **Pusch R**, **Clark W**, **Rose J**, **Güntürkün O.** Visual categories and concepts in the avian brain. *Anim Cogn* 26: 153–173, 2023. doi:10.1007/s10071-022-01711-8.
6. **Jones MP**, **Pierce KE**, **Ward D.** Avian vision: a review of form and function with special consideration to birds of prey. *J Exot Pet Med* 16: 69–87, 2007. doi:10.1053/j.jepm.2007.03.012.
7. **Bischof HJ**, **Watanabe S.** On the structure and function of the tectofugal visual pathway in laterally eyed birds. *Eur J Morphol* 35: 246–254, 1997. doi:10.1076/ejom.35.4.246.13080.
8. **Shimizu T**, **Bowers AN.** Visual circuits of the avian telencephalon: evolutionary implications. *Behav Brain Res* 98: 183–191, 1999. doi:10.1016/S0166-4328(98)00083-7.
9. **Shimizu T**, **Patton TB**, **Husband SA.** Avian visual behavior and the organization of the telencephalon. *Brain Behav Evol* 75: 204–217, 2010. doi:10.1159/000314283.
10. **Baron J**, **Pinto L**, **Dias MO**, **Lima B**, **Neuenschwander S.** Directional responses of visual wulst neurones to grating and plaid patterns in the awake owl. *Eur J Neurosci* 26: 1950–1968, 2007. doi:10.1111/j.1460-9568.2007.05783.x.
11. **Watanabe S**, **Mayer U**, **Bischof HJ.** Visual Wulst analyses "where" and entopallium analyses "what" in the zebra finch visual system. *Behav Brain Res* 222: 51–56, 2011. doi:10.1016/j.bbr.2011.03.035.
12. **Cioccarelli S**, **Giunchi D**, **Casini G**, **Pollonara E**, **Bingman VP**, **Gagliardo A.** Landscape heterogeneity and novelty drive avian oscillatory flight behaviour during forebrain Wulst-dependent visual map learning. *Proc Biol Sci* 292: 20243099, 2025. doi:10.1098/rspb.2024.3099.

13. **Remy M**, **Güntürkün O.** Retinal afferents to the tectum opticum and the nucleus opticus principalis thalami in the pigeon. *J Comp Neurol* 305: 57–70, 1991. doi:10.1002/cne.903050107.
14. **Pettigrew JD**, **Konishi M.** Neurons selective for orientation and binocular disparity in the visual wulst of the barn owl (*Tyto alba*). *Science* 193: 675–678, 1976. doi:10.1126/science.948741.
15. **Nieder A**, **Wagner H.** Horizontal-disparity tuning of neurons in the visual forebrain of the behaving barn owl. *J Neurophysiol* 83: 2967–2979, 2000. doi:10.1152/jn.2000.83.5.2967.
16. **Michael N**, **Löwel S**, **Bischof HJ.** Features of the retinotopic representation in the visual wulst of a laterally eyed bird, the zebra finch (*Taeniopygia guttata*). *PLoS One* 10: e0124917, 2015. doi:10.1371/journal.pone.0124917.
17. **Clark W**, **Colombo M.** Seeing the forest for the trees, and the ground below my beak: global and local processing in the pigeon's visual system. *Front Psychol* 13: 888528, 2022. doi:10.3389/fpsyg.2022.888528.
18. **Kröner S**, **Güntürkün O.** Afferent and efferent connections of the caudolateral neostriatum in the pigeon (*Columba livia*): a retro- and anterograde pathway tracing study. *J Comp Neurol* 407: 228–260, 1999. doi:10.1002/(sici)1096-9861(19990503)407:2<228::aid-cne6>3.0.co;2-2.
19. **Güntürkün O**, **Ströckens F**, **Ocklenburg S.** Brain lateralization: a comparative perspective. *Physiol Rev* 100: 1019–1063, 2020. doi:10.1152/physrev.00006.2019.
20. **Vallortigara G.** The evolutionary psychology of left and right: costs and benefits of lateralization. *Dev Psychobiol* 48: 418–427, 2006. doi:10.1002/dev.20166.
21. **Straight PJ**, **Gignac PM**, **Kuenzel WJ.** A histological and diceCT-derived 3D reconstruction of the avian visual thalamofugal pathway. *Sci Rep* 14: 8447, 2024. doi:10.1038/s41598-024-58788-z.
22. **Letzner S**, **Simon A**, **Güntürkün O.** Connectivity and neurochemistry of the commissura anterior of the pigeon (*Columba livia*). *J Comp Neurol* 524: 343–361, 2016. doi:10.1002/cne.23858.
23. **Güntürkün O**, **Hellmann B**, **Melsbach G**, **Prior H.** Asymmetries of representation in the visual system of pigeons. *Neuroreport* 9: 4127–4130, 1998. doi:10.1097/00001756-199812210-00023.
24. **Costalunga G**, **Kobylkov D**, **Rosa-Salva O**, **Morandi-Raikova A**, **Vallortigara G**, **Mayer U.** Responses in the left and right entopallium are differently affected by light stimulation in embryo. *iScience* 27: 109268, 2024. doi:10.1016/j.isci.2024.109268.
25. **Morandi-Raikova A**, **Danieli K**, **Lorenzi E**, **Rosa-Salva O**, **Mayer U.** Anatomical asymmetries in the tectofugal pathway of dark-incubated domestic chicks: rightwards lateralization of parvalbumin neurons in the entopallium. *Laterality* 26: 163–185, 2021. doi:10.1080/1357650X.2021.1873357.
26. **Valencia-Alfonso CE**, **Verhaal J**, **Güntürkün O.** Ascending and descending mechanisms of visual lateralization in pigeons. *Philos Trans R Soc Lond B Biol Sci* 364: 955–963, 2009. doi:10.1098/rstb.2008.0240.
27. **Rogers L**, **Bolden S.** Light-dependent development and asymmetry of visual projections. *Neurosci Lett* 121: 63–67, 1991. doi:10.1016/0304-3940(91)90650-l.
28. **Rogers L**, **Deng C.** Light experience and lateralization of the two visual pathways in the chick. *Behav Brain Res* 98: 277–287, 1999. doi:10.1016/S0166-4328(98)00094-1.
29. **Kersten Y**, **Moll FW**, **Erdle S**, **Nieder A.** Input and output connections of the crow nidopallium caudolaterale. *eNeuro* 11: ENEURO.0098-24.2024, 2024. doi:10.1523/ENEURO.0098-24.2024.
30. **Sadananda M**, **Korte S**, **Bischof HJ.** Afferentation of a caudal forebrain area activated during courtship behavior: a tracing study in the zebra finch (*Taeniopygia guttata*). *Brain Res* 1184: 108–120, 2007. doi:10.1016/j.brainres.2007.09.040.
31. **Güntürkün O.** The avian 'prefrontal cortex' and cognition. *Curr Opin Neurobiol* 15: 686–693, 2005. doi:10.1016/j.conb.2005.10.003.
32. **Nieder A.** Convergent circuit computation for categorization in the brains of primates and songbirds. *Cold Spring Harb Perspect Biol* 15: a041526, 2023. doi:10.1101/cshperspect.a041526.
33. **Güntürkün O**, **Pusch R**, **Rose J.** Why birds are smart. *Trends Cogn Sci* 28: 197–209, 2024. doi:10.1016/j.tics.2023.11.002.
34. **Emery NJ**, **Clayton NS.** The mentality of crows: convergent evolution of intelligence in corvids and apes. *Science* 306: 1903–1907, 2004. doi:10.1126/science.1098410.
35. **Veit L**, **Hartmann K**, **Nieder A.** Spatially tuned neurons in corvid nidopallium caudolaterale signal target position during visual search. *Cereb Cortex* 27: 1103–1112, 2017. doi:10.1093/cercor/bhv299.
36. **Rinnert P**, **Kirschhock ME**, **Nieder A.** Neuronal correlates of spatial working memory in the endbrain of crows. *Curr Biol* 29: 2616–2624.e4, 2019. doi:10.1016/j.cub.2019.06.060.
37. **Rinnert P**, **Nieder A.** Neural code of motor planning and execution during goal-directed movements in crows. *J Neurosci* 41: 4060–4072, 2021. doi:10.1523/JNEUROSCI.0739-20.2021.
38. **Wagener L**, **Nieder A.** Encoding of global visual motion in the nidopallium caudolaterale of behaving crows. *Eur J Neurosci* 45: 267–277, 2017. doi:10.1111/ejn.13430.
39. **Ditz HM**, **Nieder A.** Neurons selective to the number of visual items in the corvid songbird endbrain. *Proc Natl Acad Sci USA* 112: 7827–7832, 2015. doi:10.1073/pnas.1504245112.
40. **Ditz HM**, **Nieder A.** Format-dependent and format-independent representation of sequential and simultaneous numerosity in the crow endbrain. *Nat Commun* 11: 686, 2020. doi:10.1038/s41467-020-14519-2.
41. **Wagener L**, **Loconsole M**, **Ditz HM**, **Nieder A.** Neurons in the endbrain of numerically naive crows spontaneously encode visual numerosity. *Curr Biol* 28: 1090–1094.e4, 2018. doi:10.1016/j.cub.2018.02.023.
42. **Kirschhock ME**, **Nieder A.** Number selective sensorimotor neurons in the crow translate perceived numerosity into number of actions. *Nat Commun* 13: 6913, 2022. doi:10.1038/s41467-022-34457-5.
43. **Kirschhock ME**, **Nieder A.** Association neurons in the crow telencephalon link visual signs to numerical values. *Proc Natl Acad Sci USA* 120: e2313923120, 2023. doi:10.1073/pnas.2313923120.
44. **Troscianko J**, **von Bayern AMP**, **Chappell J**, **Rutz C**, **Martin GR.** Extreme binocular vision and a straight bill facilitate tool use in New Caledonian crows. *Nat Commun* 3: 1110, 2012. doi:10.1038/ncomms2111.
45. **Ditz HM**, **Nieder A.** Sensory and working memory representations of small and large numerosities in the crow endbrain. *J Neurosci* 36: 12044–12052, 2016. doi:10.1523/JNEUROSCI.1521-16.2016.
46. **Kersten Y**, **Friedrich-Müller B**, **Nieder A.** A brain atlas of the carrion crow (*Corvus corone*). *J Comp Neurol* 530: 3011–3038, 2022. doi:10.1002/cne.25392.
47. **Berens P.** CircStat: a MATLAB toolbox for circular statistics. *J Stat Soft* 31: 1–21, 2009. doi:10.18637/jss.v031.i10.
48. **Veit L**, **Hartmann K**, **Nieder A.** Neuronal correlates of visual working memory in the corvid endbrain. *J Neurosci* 34: 7778–7786, 2014. doi:10.1523/JNEUROSCI.0612-14.2014.
49. **Itahara A**, **Kano F.** Gaze tracking of large-billed crows (*Corvus macrorhynchos*) in a motion capture system. *J Exp Biol* 227: jeb246514, 2024. doi:10.1242/jeb.246514.
50. **Rahman ML**, **Sugita S**, **Aoyama M**, **Sugita S.** Number, distribution and size of retinal ganglion cells in the jungle crow (*Corvus macrorhynchos*). *Anat Sci Int* 81: 253–259, 2006. doi:10.1111/j.1447-073X.2006.00151.x.
51. **Xiao Q**, **Güntürkün O.** "Prefrontal" neuronal foundations of visual asymmetries in pigeons. *Front Physiol* 13: 882597, 2022. doi:10.3389/fphys.2022.882597.
52. **Xiao Q**, **Frost BJ.** Looming responses of telencephalic neurons in the pigeon are modulated by optic flow. *Brain Res* 1305: 40–46, 2009. doi:10.1016/j.brainres.2009.10.008.
53. **Nguyen AP**, **Spetch ML**, **Crowder NA**, **Winship IR**, **Hurd PL**, **Wylie DRW.** A dissociation of motion and spatial-pattern vision in the avian telencephalon: implications for the evolution of "visual streams". *J Neurosci* 24: 4962–4970, 2004. doi:10.1523/JNEUROSCI.0146-04.2004.
54. **Pinto L**, **Baron J.** Spatiotemporal frequency and speed tuning in the owl visual wulst. *Eur J Neurosci* 30: 1251–1268, 2009. doi:10.1111/j.1460-9568.2009.06918.x.
55. **Iwaniuk AN**, **Heesy CP**, **Hall MI**, **Wylie DRW.** Relative Wulst volume is correlated with orbit orientation and binocular visual field in birds. *J Comp Physiol A Neuroethol Sens Neural Behav Physiol* 194: 267–282, 2008. doi:10.1007/s00359-007-0304-0.
56. **Pettigrew JD.** Binocular visual processing in the owl's telencephalon. *Proc R Soc Lond B Biol Sci* 204: 435–454, 1979. doi:10.1098/rspb.1979.0038.
57. **Diekamp B**, **Kalt T**, **Ruhm A**, **Koch M**, **Güntürkün O.** Impairment in a discrimination reversal task after D1 receptor blockade in the pigeon "prefrontal cortex. *Behav Neurosci* 114: 1145–1155, 2000. doi:10.1037//0735-7044.114.6.1145.

58. **Bast T**, **Diekamp B**, **Thiel C**, **Schwarting RKW**, **Güntürkün O.** Functional aspects of dopamine metabolism in the putative prefrontal cortex analogue and striatum of pigeons (*Columba livia*). *J Comp Neurol* 446: 58–67, 2002. doi:10.1002/cne.10187.
59. **Martinez-Trujillo J.** Visual attention in the prefrontal cortex. *Annu Rev Vis Sci* 8: 407–425, 2022. doi:10.1146/annurev-vision-100720-031711.
60. **Brecht KF**, **Westendorff S**, **Nieder A.** Neural correlates of cognitively controlled vocalizations in a corvid songbird. *Cell Rep* 42: 112113, 2023. doi:10.1016/j.celrep.2023.112113.
61. **Packheiser J**, **Donoso JR**, **Cheng S**, **Güntürkün O**, **Pusch R.** Trial-by-trial dynamics of reward prediction error-associated signals during extinction learning and renewal. *Prog Neurobiol* 197: 101901, 2021. doi:10.1016/j.pneurobio.2020.101901.
62. **Johnston M**, **Brecht KF**, **Nieder A.** Crows flexibly apply statistical inferences based on previous experience. *Curr Biol* 33: 3238–3243.e3, 2023. doi:10.1016/j.cub.2023.06.023.
63. **Yamamoto K**, **Furuya I**, **Watanabe S.** Near-field visual acuity in Japanese jungle crows (*Corvus macrorhynchos*). *Physiol Behav* 72: 283–286, 2001. doi:10.1016/S0031-9384(00)00356-5.
64. **Caves EM**, **Fernández-Juricic E**, **Kelley LA.** Ecological and morphological correlates of visual acuity in birds. *J Exp Biol* 227: jeb246063, 2024. doi:10.1242/jeb.246063.
65. **Heimel JA**, **Van Hooser SD**, **Nelson SB.** Laminar organization of response properties in primary visual cortex of the gray squirrel (*Sciurus carolinensis*). *J Neurophysiol* 94: 3538–3554, 2005. doi:10.1152/jn.00106.2005.
66. **Benmazouz I**, **Jokimäki J**, **Lengyel S**, **Juhász L**, **Kaisanlahti-Jokimäki ML**, **Kardos G**, **Paládi P**, **Kövér L.** Corvids in urban environments: a systematic global literature review. *Animals (Basel)* 11: 3226, 2021. doi:10.3390/ani11113226.
67. **Nixdorf BE**, **Bischof HJ.** Afferent connections of the ectostriatum and visual wulst in the zebra finch (Taeniopygia guttata castanotis Gould)—an HRP study. *Brain Res* 248: 9–17, 1982. doi:10.1016/0006-8993(82)91142-8.
68. **Verhaal J**, **Kirsch JA**, **Vlachos I**, **Manns M**, **Güntürkün O.** Lateralized reward-related visual discrimination in the avian entopallium. *Eur J Neurosci* 35: 1337–1343, 2012. doi:10.1111/j.1460-9568.2012.08049.x.
69. **Manns M**, **Ströckens F.** Functional and structural comparison of visual lateralization in birds—similar but still different. *Front Psychol* 5: 206), 2014. doi:10.3389/fpsyg.2014.00206.
70. **Hahner L**, **Nieder A.** Volitional spatial attention is lateralized in crows. *Proc Biol Sci* 292: 20242540, 2025. doi:10.1098/rspb.2024.2540.